Journal of Maps

ISSN: (Print) (Online) Journal homepage: https://www.tandfonline.com/loi/tjom20

# Morphostructural mapping of Borealis Planitia, Mercury

Marco Cardinale, David A. Vaz, Piero D'Incecco, Nicola Mari, Justin Filiberto, Gabriel L. Eggers & Gaetano Di Achille

**To cite this article:** Marco Cardinale, David A. Vaz, Piero D'Incecco, Nicola Mari, Justin Filiberto, Gabriel L. Eggers & Gaetano Di Achille (2023) Morphostructural mapping of Borealis Planitia, Mercury, Journal of Maps, 19:1, 2223637, DOI: 10.1080/17445647.2023.2223637

**To link to this article:** https://doi.org/10.1080/17445647.2023.2223637

JOURNAL OF MAPS
2023, VOL. 19, NO. 1, 2223637
https://doi.org/10.1080/17445647.2023.2223637

Taylor & Francis
Taylor & Francis Group

Science



# Morphostructural mapping of Borealis Planitia, Mercury

Marco Cardinale[a], David A. Vaz[b], Piero D'Incecco[a], Nicola Mari[c], Justin Filiberto[d], Gabriel L. Eggers[e] and Gaetano Di Achille [a]

[a]National Institute for Astrophysics, Astronomical Observatory of Abruzzo, Teramo, Italy; [b]Centre for Earth and Space Research of the University of Coimbra, Observatório Geofísico e Astronómico da Universidade de Coimbra, Coimbra, Portugal; [c]Dipartimento di Scienze della Terra e dell'Ambiente, University of Pavia, Pavia, Italy; [d]Astromaterials Research and Exploration (ARES) Division, X13, NASA Johnson Space Center, Houston, TX, USA; [e]Lunar and Planetary Institute, USRA, Houston, TX, USA

**ABSTRACT**

Orbital data from the MESSENGER spacecraft show that a significant portion of Mercury's northern hemisphere is covered by smooth plains, which are interpreted to be flood volcanic material and/or impact melt. The smooth plains show pervasive tectonic structures and encompass a broad raised bulge of uncertain geophysical interpretation. In this work, we focus on the mapping of all the morphostructures within the northern smooth plains, aiming at providing a useful dataset for further studies about the mapped area. The structural map is obtained through a twofold process: first with an automatic mapping, using an algorithm to identify all the lineaments from a DEM; and second with a visual inspection and classification of the results of the algorithm in a GIS environment. The final maps are drafted at two different scales, 1:300,000 and 1:600,000. With this approach, we mapped and characterized more than fifty thousand lines marking scarps on the surface, creating a database with several morphometric attributes for each of the identified scarps (e.g. length, azimuth, and height), which can be used for geostatistical study of smooth plains tectonics. Our structural map reveals that: (i) the area is broadly dominated by wrinkle ridges, ghost crater assemblages of lineaments, and scarps related to impact crater processes (e.g. radial faults, secondary crater chains, ejecta emplacement) and that (ii) the amount of strain was not evenly accommodated throughout the northern smooth plains.

**ARTICLE HISTORY**
Received 22 December 2022
Revised 5 May 2023
Accepted 17 May 2023

**KEYWORDS**
Mercury; wrinkle ridges; ghost craters; automatic mapping; tectonic processes

## 1. Introduction

Orbital data acquired by the Mercury Dual Imaging System (MDIS) instrument onboard the NASA MESSENGER (Mercury Surface, Space Environment, Geochemistry, and Ranging) mission (Solomon Sean, et al., 2001, 2008) enabled the completion of the first mapping of Mercury's north polar region (50–90° of latitude). Previously, Mariner 10 and MESSENGER flyby image coverage (Danielson et al., 1975; Solomon et al., 2008; Trask & Guest, 1975) showed large regions of smooth plains surrounded by cratered terrains (Denevi et al., 2009; Head et al., 2011; Spudis & Guest, 1988; Strom et al., 2008). New orbital data acquired by MDIS (Hawkins et al., 2007) provided full coverage of the northern region of Mercury at high resolution, allowing a better understanding of the geomorphology of the area.

Two main geological terrains characterize the Mercury's north polar region: the northern heavily cratered terrain (NHCT) and the northern smooth plains (NSP) (Ostrach et al., 2015). The first unit is characterized by densely cratered areas (Fassett et al., 2011; Trask & Guest, 1975). The northern smooth plains are instead uniform with far fewer craters than the cratered terrain (Guest & Gault, 1976; Strom et al., 1975) and geomorphological features similar to the lunar maria (Head et al., 2008, p. 2011; Strom et al., 1975), though with different composition (e.g. Nittler et al., 2011; Vander Kaaden et al., 2017). Mariner 10 imagery showed that the NSP have a lower density of impact craters and are younger than the NHCT (Denevi et al., 2009; Head et al., 2011; Strom et al., 1975, p. 1975). The limited spatial resolution of the Mariner 10 dataset (Malin, 1978; Milkovich et al., 2002) did not permit the identification of volcanic features, but a volcanic origin of the NSP was hypothesized due to their distribution, young age, visible color properties, and overlapping relationships with tectonic structures (Murray, 1975; Robinson & Lucey, 1997; Robinson & Taylor, 2001; Spudis & Guest, 1988). It is also possible that the NSP are widely distributed due to effusive volcanism (Byrne et al., 2013; Denevi et al., 2009, 2013; Fassett et al., 2009; Freed et al., 2012; Goudge et al., 2014; Head et al., 2008, 2009, p. 2011; Hurwitz et al., 2013; Kerber et al., 2009, 2011; Klimczak et al., 2012; Murchie et al., 2008; Robinson

CONTACT Gaetano Di Achille gaetano.diachille@inaf.it National Institute for Astrophysics (INAF), Astrnomical Observatory of Abruzzo, Teramo, Italy
Supplemental map for this article is available online at https://doi.org/10.1080/17445647.2023.2223637.

et al., 2008; Solomon et al., 2008). Furthermore, volcanic activity in the NSP could be related to phenomena of partial flooding of the crater floors (Head et al., 2009) or to the record of volcanically resurfaced impact crater regions (Ostrach et al., 2015). Finally, the NSP area is characterized by the widespread occurrence of morphologic scarps as investigated in previous studies about the tectonics of the region based on digital mapping (e.g. Crane & Klimczak, 2019).

Significant improvements in digital mapping procedures and new photo interpretation techniques along with the availability of high-resolution datasets have greatly improved the analysis of planetary surfaces. Several automatic mapping methods have been applied in planetary sciences to characterize geomorphologic features such as aeolian bedforms at different scales (Borraccini et al., 2007; Cardinale et al., 2020; Foroutan & Zimbelman, 2017; Vaz and Silvestro, 2014; Vaz et al., 2015); crater counting (Bandeira et al., 2007; Bue & Stepinski, 2006); and drainage networks (Stepinski & Collier, 2004). Here, we use the mapping technique introduced by Vaz (2011): a method aimed at extracting lineaments that represent topographic discontinuities from digital elevation models (DEM), which can be used to characterize tectonic structures in planetary surfaces (Vaz et al., 2014) without being affected by possible bias due to the illumination conditions of imagery.

In this work we apply this semi-automatic approach described in Vaz et al. (2014) to Mercury for the first time, producing a detailed morphotectonic map of the Borealis Planitia region. We defined our mapping area following the boundaries of the northern smooth deposits (NSP) as in Denevi et al. (2009 and 2013). Substantial parts of NSP are included in Mercury quadrangles H02 (Victoria) and H05 (Hokusai) both of which have been geologically mapped at 1:3M (Galluzzi et al., 2016; Wright et al., 2019) We adopt a semi-automatic procedure based on a digital elevation model (DEM) rather than imagery, resulting in the identification of tens of thousands of structures within the NSP (Figure 1), which represents a significantly wider geodatabase with respect to the previous maps obtained using traditional mapping techniques (e.g. Crane & Klimczak, 2019). The numeric attributes of each of the mapped lineaments can be used for quantitative studies to better characterize the density and spatial distribution of tectonic features and improve our understanding of the tectonic evolution of the NSP. Finally, Mercury's structural maps derived from imagery photogeologic interpretation might often be biased by the variable resolution and illumination conditions of the used basemaps. Indeed, more recent investigations based on MESSENGER data (Solomon et al., 2008), led to the revision of previous results based on Mariner imagery (e.g. Di Achille et al., 2012; Watters & Nimmo, 2010; Watters et al., 1998, 2004, 2009). In contrast, our mapping approach is unaffected by the imagery illumination conditions and variable resolution, since it is based on the use of a fixed resolution datasets, such as a equally spaced DEM.

## 2. Data and methods

MESSENGER MDIS visible imagery (Denevi et al., 2016; Hawkins et al., 2007) with a resolution of 166 meters per pixel was used as a basemap. Topography was reprocessed using the raw Mercury Laser Altimeter (MLA) data (Denevi et al., 2016; Hawkins et al., 2007), creating a final DEM with 500 m/pix to better characterize the tectonic lineaments and measure morphometric parameters (e.g. length, azimuth, scarp height). Elevation points were integrated using a block median operator (Wessel & Smith, 1998), and a natural neighbor algorithm was used for the interpolation. The first iteration revealed that some of the orbits presented a noticeable vertical offset. Therefore, we identified and removed 128 orbits from the dataset, obtaining a more uniform DEM.

With these datasets, we implemented a Geographical Information System (GIS) project in stereographic projection (centered at the NSP, 70° N and 30° E) and created a geo-structural map of the surface (Figures 2 and 3). Our map is obtained through a twofold process: (1) automatic mapping using an algorithm to identify all the lineaments from a DEM (Vaz, 2011; Vaz et al., 2014), and (2) visual inspection and classification of the results in a GIS environment. The final maps were drafted at two different scales, 1:300,000 and 1:600,000. With this approach, we mapped and characterized more than fifty thousand lines marking tectonic features on the surface, creating a database with several morphometric attributes (e.g. length, azimuth, tectonic lineaments height – a list of all the derived parameters and their description is provided in the Supplementary materials) that can be used for the geostatistical study of the smooth plains' tectonics. With respect to traditional mapping based on visible interpretation of imagery and topography, the technique used in this work is a more robust and detailed approach since it recognizes and maps all scarps present in the DEM; however, this means that a scarp/lineament classification stage is needed in order to study a specific set/type of structure. This is achieved through the second mapping step (the visual inspection of the results of the automatic procedure) by overlaying the mapped lineaments onto the image mosaics in a GIS interface, allowing a user to interpret the geomorphological meaning/origin of the automatically mapped features. In this classification stage, we recognized the tectonic structures and excluded other features that were not relevant for the structural analysis, some of which were not recognizable in the imagery or were clearly associated with DEM

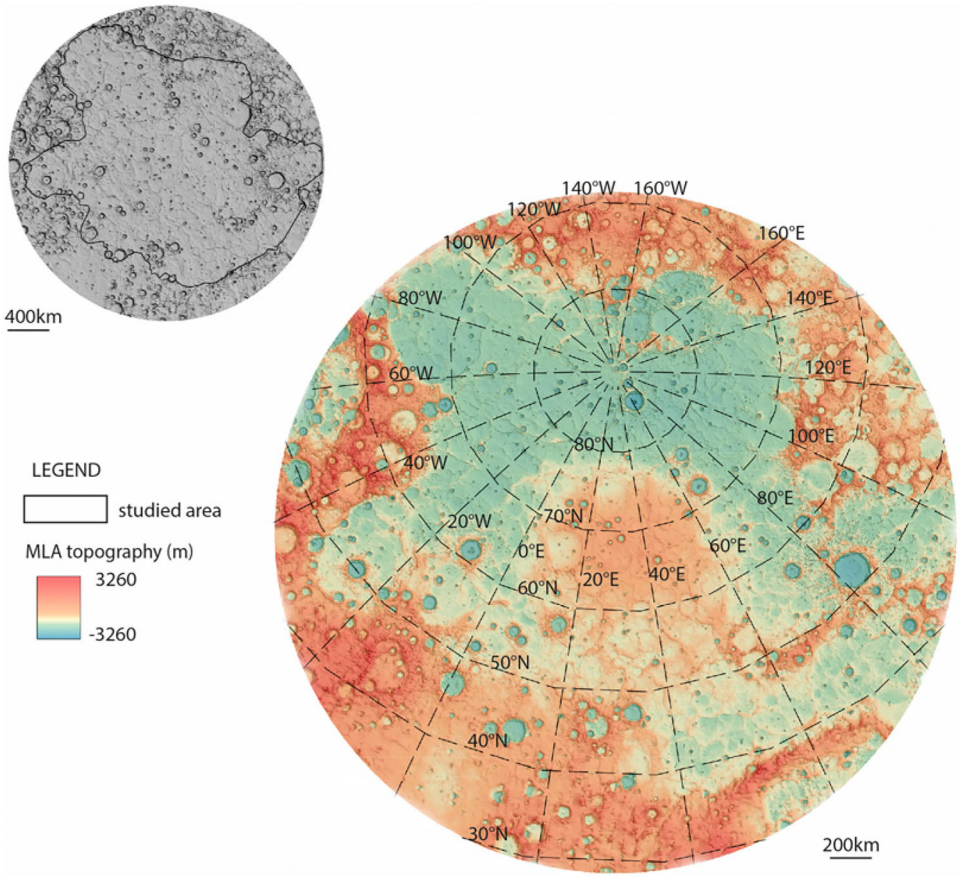


**Figure 1.** Northern hemisphere of Mercury: color coding from MLA topography. The investigated area is outlined by the black contour in the upper left inset.

artifacts. In this way, we extracted 45,012 lines from the DEM (Figure 2) and classified them as wrinkle ridges, lobate scarps, ghost craters, craters, and crater ejecta.

The same methods have previously been validated with MOLA (Mars Orbiter Laser Altimeter, 231 m/pixel) data and proved to be an effective way to map and analyze tectonic morphologies on other planets, producing tectono-structural maps that are comparable to photointerpretations (Vaz et al., 2012). We then investigated the regional stress fields using the orientation of the mapped tectonic lines, representing them in a rose diagram and computing circular statistics (Figure 4). Finally, we present line density maps weighted by the length and by the average height of the scarps computed on a circular kernel with 100 km radius (Figure 5). Particularly, we extracted a line density maps for the tectonic structures (Figure 5(a)) and a density map weighted for the product of line length by line height (Figure 5(b)).

## 3. Results

We divided the identified lineaments into the following units: tectonic lines (e.g. wrinkle ridges, lobate scarps), ghost craters (buried and/or subdued impact craters with circular outlines) still visible in the elevation data as annular ridges; Head et al., 2009), craters (rims and central peaks), and crater ejecta (materials excavated from a crater cavity during impact or erupted from a volcanic vent – Hargitai, 2021). The photo-interpretation and inspection of the automatically identified features resulted in the exclusion of about 5% of the original lineaments, reducing the final identified lineaments to about 45,000 (Figure 2). The excluded lineaments were mostly represented by small (few kilometer long) elements that could not be associated to any of the defined structural units based on visual inspection of images and topography and their geological context. These lineaments were most likely due to DEM artifacts at km-scale. Within the investigated area, 27.5% of the mapped features correspond to tectonic features (wrinkle ridges and lobate scarps), 4.3% to ghost craters, 24.7% to craters, and 43.5% to crater ejecta. Tectonic features are spread over the entire area (Figures 3(a)–(b)) with lengths ranging between 4 and 180 km. The mapped scarps form complex arrays of wrinkle ridges and lobate scarps with average height of 245 ± 131 m. We also mapped ghost craters (Figure 3(a)–(b)). These features are widespread throughout the NSP area and outline impact features with diameters ranging from a few to several hundreds of kilometers (Figure 3(a)). The largest basin (Figure 3(a)) within the studied area, near Borealis Planitia, has a diameter of about 200 km and may contain graben structures in the crater floor (Head et al., 2011). In this area, we also mapped craters with diameters ranging between

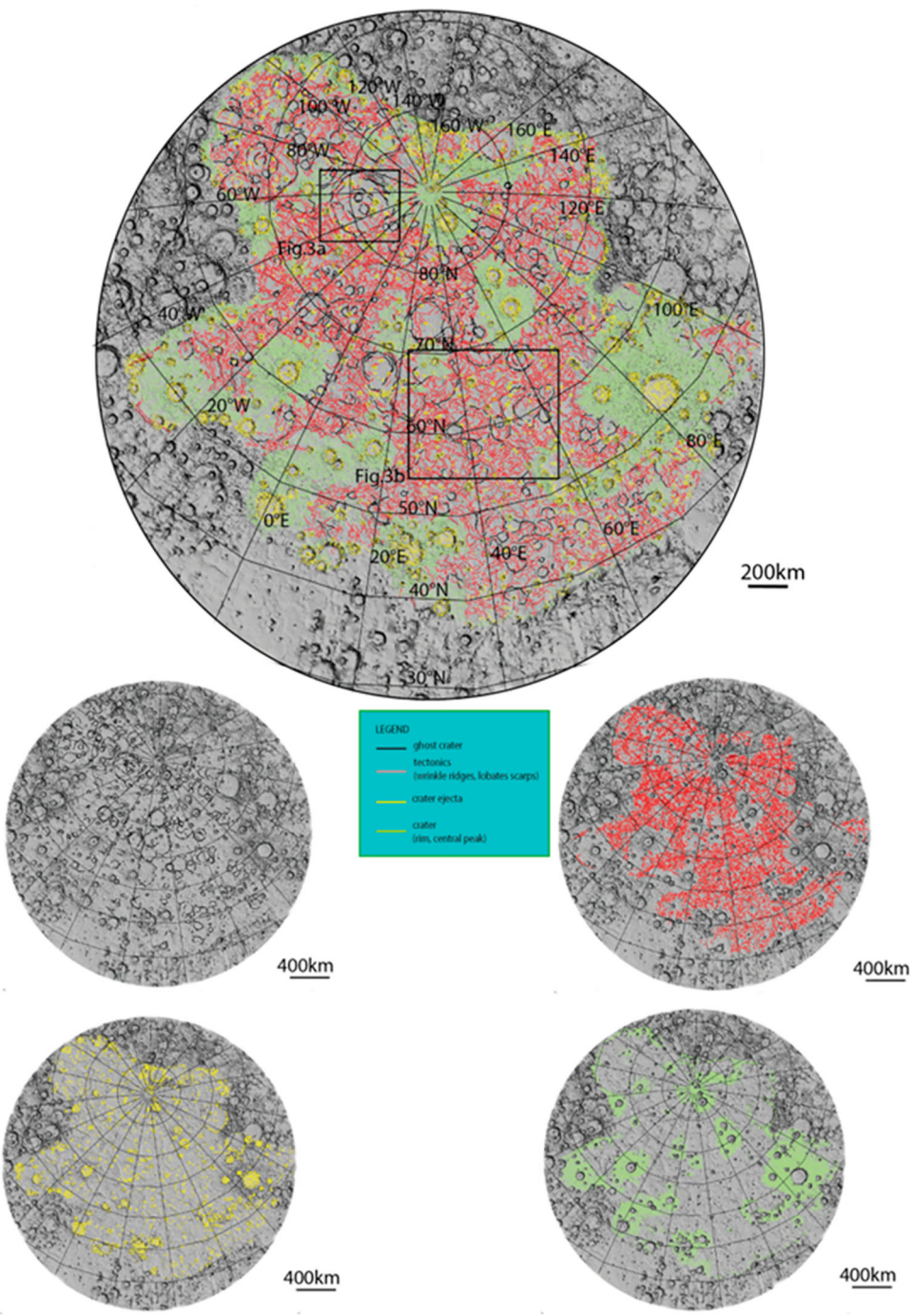


**Figure 2.** MLA shaded relief with superimposed geo-structural map. Lines were automatically extracted from the DTM and manually classified according to their geomorphologic significance using visible image mosaics for context.

80 and 200 km (Figure 3), including both rims and central peaks in the same class. A separate unit has been defined for the crater ejecta (Figure 3).

An overview of the lineament density map (Figure 5(a)) does not show clear tectonic clusters. The overall spatial anisotropy of the features shows a few gaps occurring in the central zone of the map. These gaps are related to the obliteration of features by impact crater structures since the gaps are associated with relatively young craters showing well-developed ejecta blankets (compare Figure 2 and Figure 5(a)). However, at the regional scale several high spatial density zones are localized in association with topographic rises and ghost craters. Contrary to the homogeneity of the spatial distribution of the lineaments, a plot of the Cartesian azimuth of the structural features shows a clear bimodal distribution at ~50° and ~135° (Figure 4). It is unclear whether the latter bimodal distribution might be related to a global stress field compatible with the overall geodynamic evolution of Mercury (e.g. Di Achille et al., 2012; Dombard, and Hauck, 2008; Melosh & Dzurisin, 1978). In addition, more detailed observations are needed to evaluate the different hypotheses to explain the tectonic evolution of Mercury's northern smooth plains. Standard line density (obtained by dividing the partial length of

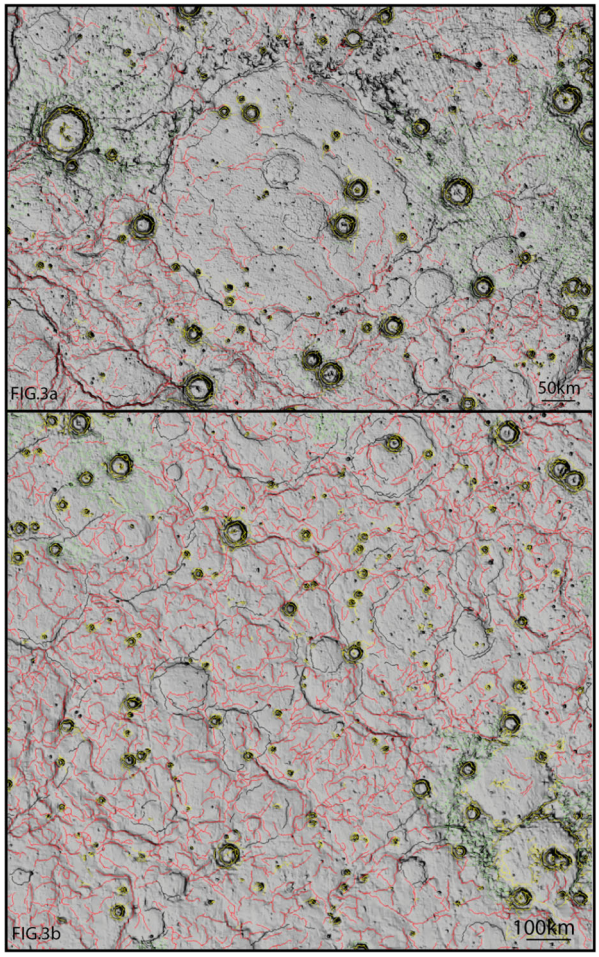


**Figure 3.** Close up of two regions (see Figure 2 for locations) within the studied area, showing the mapped features based on the photo-interpretation of DEM and visible data.

the lines that intersect the circular sampling neighborhood and its area) is nearly uniform, excluding the areas where craters and their ejecta obscure the tectonic features (Figure 5(a)). However, the line density weighted by the average height of the tectonic scarps; i.e. the density that is weighted by the length*height product and represents the vertical area deformed by the tectonic processes, suggests that strains are not uniform, with higher strains concentrated north-northwest of the bulge. Indeed, the latter weighting parameterization is a better proxy for the amount of cumulative strain since it integrates 3D information usually not considered in the classic 2D analysis of tectonic lineaments.

Finally, we could not quantitatively compare our results to previous mapping studies (e.g. Crane & Klimczak, 2019; Galluzzi et al., 2016; Wright et al., 2019) within the Borealis Planitia since none of the published maps were publicly released in GIS format. Moreover, Wright et al. (2019) and Galluzzi et al. (2016) focused their mapping mostly on geological units, classifying main tectonic structures at the mapped scale. While Crane and Klimczak (2019) focused their mapping on the tectonic structures of Borealis Planitia following standard mapping approaches based on visual inspection of datasets. They reported a main E-W trend for wrinkle ridges. Our results do not confirm the presence of such E-W preferential orientation for wrinkle ridges. This inconsistency might be explained considering the different mapping approaches and the

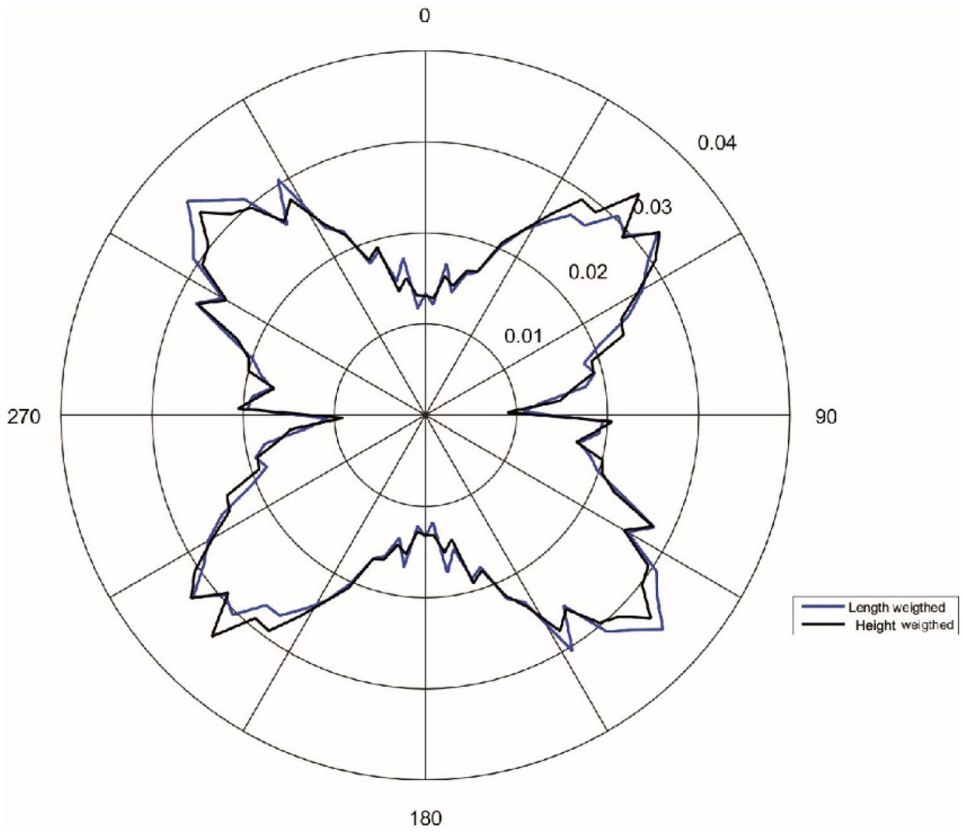


**Figure 4.** Scarps length- (blue) and height- (black) -weighted azimuth frequency distribution of the tectonic features.

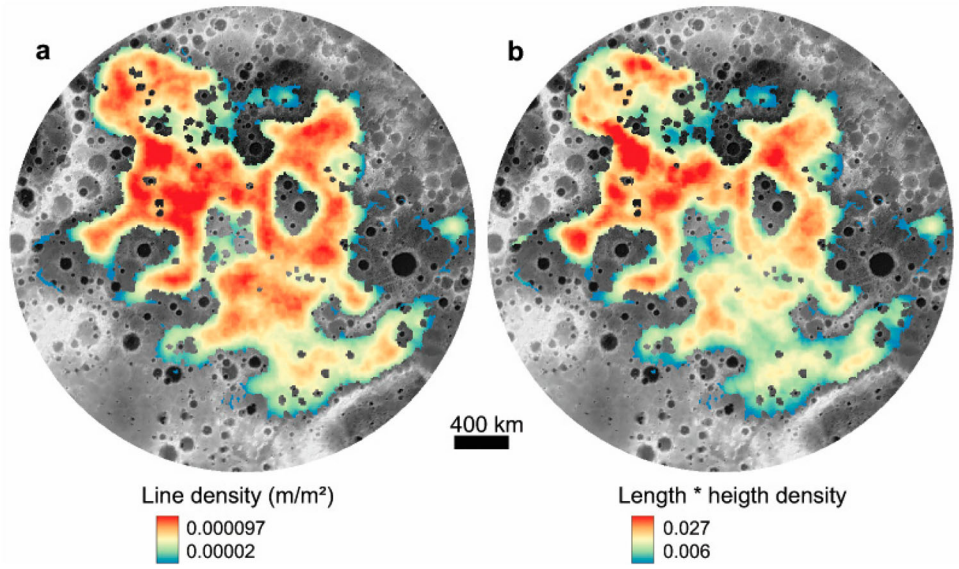


**Figure 5.** Line density of the mapped tectonic features computed on a circular kernel with 100 km radius. (a) standard line density (obtained by dividing the partial length of the lines that intersect the circular sampling neighborhood and its area); excluding the areas where craters and their ejecta obscure the tectonic features the density distribution is nearly uniform. (b) line density weighted by the average height of the tectonic scarps, i.e. the density is weighted by the length*height product, which represents the vertical area deformed by the tectonic processes; this parameterization is a better proxy for the amount of cumulative strain, since it integrates 3D information usually not considered in the classic 2D analysis of tectonic lineaments. Overall, the data suggests that strains are not uniform, with higher strains concentrated north-northwest of the bulge.

possibility that the E-W trend reported by Crane and Klimczak (2019) might have been biased by the imagery illumination conditions in relationship with the sub-vertical inclination of the Mercury's axis that would enhance the visibility of E-W oriented structures.

## 4. Summary

We present a high-resolution structural map of the Mercury's northern smooth plains produced using a semi-automatic mapping approach based on a tailored DEM. The new map revealed more than 45,000 morphotectonic lineaments over the northern smooth plains of Mercury. The identified lineaments have been archived into GIS vector shapefiles, including several numeric attributes (e.g. azimuth, length, height, slope, etc.) for each lineament. These morphometric attributes allowed us to characterize the spatial distribution of tectonic lineaments, which can be used to perform tectonic structural studies about the NSP. This map reveals that the area is broadly dominated by wrinkle ridges, ghost crater assemblages of lineaments, and scarps related to impact crater processes (e.g. radial faults, secondary crater chains, ejecta emplacement). Our structural regional analysis may be used as basemap for tectonic and geodynamic studies to understand the evolution of the northern smooth plains, as well as a target database for future missions to Mercury, starting with the joint ESA-JAXA BepiColombo mission.

## Software

The tailored DEM used in this study was derived reprocessing MESSENGER Mercury Laser Altimeter (MLA) data (Denevi et al., 2016; Hawkins et al., 2007), by integrating the elevation points using the software Generic Mapping Tool (GMT, Wessel & Smith, 1998) and its block median operator. MESSENGER MDIS visible imagery (Denevi et al., 2016; Hawkins et al., 2007) were processed and mosaicked using the USGS Astrogeology Research Program Integrated Software for Imagers and Spectrometers (ISIS, http://isis.astrogeology.usgs.gov) software. Imagery and topography were subsequently used to implement a Geographical Information System (GIS) project using the QGIS software (http://www.qgis.org). The automatic mapping was realized with an algorithm to identify all the lineaments from a DEM (Vaz, 2011; Vaz et al., 2014) using the MATLAB software and exported as linear Shapefile. The final maps were drafted in QGIS using its Shapefile and layout editing tools.

## Acknowledgments

We thank D. A. Rothery, V. Galluzzi, and Vit Paszto for the constructive reviews.

## Open Scholarship

This article has earned the Center for Open Science badge for Open Data. The data are openly accessible at 10.57760/sciencedb.06982.

This article has earned the Center for Open Science badge for Open Materials. The data are openly accessible at 10.57760/sciencedb.06982.

## Disclosure statement

No potential conflict of interest was reported by the author(s).

## Funding

This work was supported by the Italian Space Agency (ASI) under Grants [2017-40-H.1-2020] and [2022-16-HH.0].

## Data availability statement

The authors confirm that the data supporting the findings of this study are available within the article and its supplementary materials.

## ORCID

*Gaetano Di Achille* http://orcid.org/0000-0002-2151-4057

## References

Bandeira, L., Saraiva, J., & Pina, P. (2007). Impact crater recognition on Mars based on a probability volume created by template matching. *IEEE Transactions on Geoscience and Remote Sensing*, *45*(12), 4008–4015. https://doi.org/10.1109/TGRS.2007.904948

Borraccini, F., Di Achille, G., Ori, G. G., & Wezel, F. C. (2007). Tectonic evolution of the eastern margin of the thaumasia plateau (Mars) as inferred from detailed structural mapping and analysis. *Journal of Geophysical Research*, *112*. Http://dx.doi.og/10.10292006JE002866

Bue, B. D., & Stepinski, T. F. (2006). Automated classification of landforms on Mars. *Computers & Geosciences*, *32*, 604–614.

Byrne, P. K., Christian, K., David, A. W., Debra, M. H., Sean, C. S., James, W. H., Frank, P., & Jürgen, O. (2013). An assemblage of lava flow features on Mercury. *Journal of Geophysical Research: Planets*, *118*(6), 1303–1322. https://doi.org/10.1002/jgre.20052

Cardinale, M., Pozzobon, R., Tangari, A. C., Runyon, K., Di Primio, M., & Marinangeli, L. (2020). Reconstruction of the sand transport pathways and provenance in moreux crater, Mars. *Planetary and Space Science*, *181*, Article 104788. https://doi.org/10.1016/j.pss.2019.104788

Crane, K. T., & Klimczak, C. (2019). Tectonic patterns of shortening landforms in Mercury's northern smooth plains. *Icarus*, *317*, 66–80. https://doi.org/10.1016/j.icarus.2018.05.034

Danielson, G. E., Klaasen, K. P., & Anderson, J. L. (1975). Acquisition and description of mariner 10 television science data at mercury. *Journal of Geophysical Research*, *80*(17), 2357–2393. https://doi.org/10.1029/JB080i017p02357.

Denevi, B. W., Ernst, C. M., Meyer, H. M., Robinson, M. S., Murchie, S. L., Whitten, J. L., Head, J. W., Watters, T. R., Solomon, S. C., Ostrach, L. R., Chapman, C. R., Byrne, P. K., Klimczak, C., & Peplowski, P. N. (2013). The distribution and origin of smooth plains on Mercury. *Journal of Geophysical Research: Planets*, *118*(5), 891–907. https://doi.org/10.1002/jgre.20075

Denevi, B. W., Frank, P. S., Ernst, C. M., Keller, M. R., Chabot, N. L., Murchie, S. L., Domingue, D. L., Hash, C. D., & Blewett, D. T. (2016). Final calibration and multispectral map products from the mercury dual imaging system wide-angle camera on MESSENGER. *Lunar and Planetary Science Conference*, *47*, abstract #1264.

Denevi, B. W., Robinson, M. S., Solomon, S. C., Murchie, S. L., Blewett, D. T., Domingue, D. L., McCoy, T. J., Ernst, C. M., Head, J. W., Watters, T. R., & Chabot, N. L. (2009). The evolution of Mercury's crust: A global perspective from MESSENGER. *Science*, *324*, 613–618. https://doi.org/10.1126/science.1172226.

Di Achille, G., Popa, C., Massironi, M., Epifani, E. M., Zusi, M., Cremonese, G., & Palumbo, P. (2012). Mercury's radius change estimates revisited using MESSENGER data. *Icarus*, *221*(1), 456–460. https://doi.org/10.1016/j.icarus.2012.07.005

Dombard, A. J., & Hauck, S. A. (2008). Despinning plus global contraction and the orientation of lobate scarps on Mercury: Predictions for MESSENGER. *Icarus*, *198*(1), 274–276. https://doi.org/10.1016/j.icarus.2008.06.008

Fassett, C. I., Head, J. W., Blewett, D. T., Chapman, C. R., Dickson, J. L., Murchie, S. L., Solomon, S. C., & Watters, T. R. (2009). Caloris impact basin: Exterior geomorphology, stratigraphy, morphometry, radial sculpture, and smooth plains deposits. *Earth and Planetary Science Letters*, *285*(3-4), 297–308. https://doi.org/10.1016/j.epsl.2009.05.022

Fassett, C. I., Kadish, S. J., Head, J. W., Solomon, S. C., & Strom, R. G. (2011). The global population of large craters on Mercury and comparison with the Moon. *Geophysical Research Letters*, *38*, L10202. https://doi.org/10.1029/2011GL047294

Foroutan, M., & Zimbelman, J. R. (2017). Semi-automatic mapping of linear-trending bedforms using 'self-organizing maps' algorithm. *Geomorphology*, *293*, 156–166. https://doi.org/10.1016/j.geomorph.2017.05.016

Freed, A. M., Blair, D. M., Watters, T. R., Klimczak, C., Byrne, P. K., Solomon, S. C., Zuber, M. T., & Melosh, H. J. (2012). On the origin of graben and ridges within and near volcanically buried craters and basins in Mercury's northern plains. *Journal of Geophysical Research: Planets*, *117*, E00L–E006. https://doi.org/10.1029/2012JE004119

Galluzzi, V., Guzzetta, L., Ferranti, F., Di Achille, G., Rothery, D. A., & Palumbo, P. (2016). Geology of the Victoria quadrangle (H02), Mercury. *Journal of Maps*, *12*(sup1), 227–238. https://doi.org/10.1080/17445647.2016.1193777

Goudge, T. A., Head, J. W., Kerber, L., Blewett, D. T., Denevi, B. W., Domingue, D. L., Gillis-Davis, J. J., Gwinner, K., Helbert, J., Holsclaw, G. M., Izenberg, N. R., Klima, R. L., McClintock, W. E., Murchie, S. L., Neumann, G. A., Smith, D. E., Strom, R. G., Xiao, Z., Zuber, M. T., & Solomon, S. C. (2014). Global inventory and characterization of pyroclastic deposits on Mercury: New insights into pyroclastic activity from MESSENGER orbital data. *Journal of Geophysical Research: Planets*, *119*(3), 635–658. https://doi.org/10.1002/2013JE004480

Guest, J. E., & Gault, D. E. (1976). Crater populations in the early history of Mercury. *Geophysical Research Letters*, *3*(3), 121–123. https://doi.org/10.1029/GL003i003p00121

Hargitai, H. (2021). Ejecta deposit. In *Encyclopedia of planetary landforms*. Springer. https://doi.org/10.1007/978-1-4614-9213-9_648-1.

Hawkins, S. E., Boldt, J. D., Darlington, E. H., Espiritu, R., Gold, R. E., Gotwols, B., Grey Matthew, P., Hash Christopher, D., Hayes John, R., Jaskulek Steven, E., Kardian Charles, J., Keller Mary, R., Malaret Erick, R., Murchie Scott, L., Murphy Patricia, K., Keith, P., Louise M., P., Alan, R. R., Mark, S. R., … Bruce, D. W. (2007). The Mercury dual imaging system on the MESSENGER spacecraft. *Space Science Reviews*, *131*(1), 247–338. https://doi.org/10.1007/s11214-007-9266-3

Head, J. W., Chapman, C. R., Strom, R. G., Fassett, C. I., Denevi, B. W., Blewett, D. T., Ernst, C. M., Watters, T. R., Solomon, S. C., Murchie, S. L., Prockter, L. M., Chabot, N. L., Gillis-Davis, J. J., Whitten, J. L., Goudge, T. A., Baker, D. M. H., Hurwitz, D. M., Ostrach, L. R., Xiao, Z., … Nittler, L. R. (2011). Flood volcanism in the northern high latitudes of mercury revealed by MESSENGER. *Science*, *333*(6051), 1853–1856. https://doi.org/10.1126/science.1211997

Head, J. W., Murchie, S. L., Prockter, L. M., Robinson, M. S., Solomon, S. C., Strom, R. G., Chapman, C. R., Watters, T. R., McClintock, W. E., Blewett, D. T., & Gillis-Davis, J. J. (2008). Volcanism on Mercury: Evidence from the first MESSENGER flyby. *Science*, *321*(5885), 69–72. https://doi.org/10.1126/science.1159256

Head, J. W., Murchie, S. L., Prockter, L. M., Solomon, S. C., Chapman, C. R., Strom, R. G., Watters, T. R., Blewett, D. T., Gillis-Davis, J. J., Fassett, C. I., Dickson, J. L., Morgan, G. A., & Kerber, L. (2009). Volcanism on Mercury: Evidence from the first MESSENGER flyby for extrusive and explosive activity and the volcanic origin of plains. *Earth and Planetary Science Letters*, *285*(3-4), 227–242. https://doi.org/10.1016/j.epsl.2009.03.007

Hurwitz, D. M., Head, J. W., Byrne, P. K., Xiao, Z., Solomon, S. C., Zuber, M. T., Smith, D. E., & Neumann, G. A. (2013). Investigating the origin of candidate lava channels on Mercury with MESSENGER data: Theory and observations. *Journal of Geophysical Research: Planets*, *118*(3), 471–486. https://doi.org/10.1029/2012JE004103

Kerber, L. A., Head, J. W., Blewett, D. T., Solomon, S. C., Wilson, L., Murchie, S. L., Robinson, M. S., Denevi, B. W., & Domingue, D. L. (2011). The global distribution of pyroclastic deposits on Mercury: The view from MESSENGER flybys 1–3. *Planetary and Space Science*, *59* (15), 1895–1909. https://doi.org/10.1016/j.pss.2011.03.020

Kerber, L. A., Head, J. W., Solomon, S. C., Murchie, S. L., Blewett, D. T., & Wilson, L. (2009). Explosive volcanic eruptions on Mercury: Eruption conditions, magma volatile content, and implications for interior volatile abundances. *Earth and Planetary Science Letters*, *285*(3-4), 263–271. https://doi.org/10.1016/j.epsl.2009.04.037

Klimczak, C., Watters, T. R., Ernst, C. M., Freed, A. M., Byrne, P. K., Solomon, S. C., Blair, D. M., & Head, J. W. (2012). Deformation associated with ghost craters and basins in volcanic smooth plains on Mercury: Strain analysis and implications for plains evolution. *Journal of Geophysical Research: Planets*, *117*(E12), E00L–E003. https://doi.org/10.1029/2012JE004100

Malin, M. C. (1978). Surfaces of Mercury and the Moon: Effects of resolution and lighting conditions on the discrimination of volcanic features. *Proceedings of the Lunar Planet Science Conference*, *9*, 3395–3409.

Melosh, H. J., & Dzurisin, D. (1978). Mercurian global tectonics: A consequence of tidal despinning? *Icarus*, *35*(2), 227–236. https://doi.org/10.1016/0019-1035(78)90007-6

Milkovich, S. M., Head, J. W., & Wilson, L. (2002). Identification of mercurian volcanism: Resolution effects and implications for MESSENGER. *Meteoritics & Planetary Science*, *37*(9), 1209–1222. https://doi.org/10.1111/j.1945-5100.2002.tb00890.x

Murchie, S. L., Watters, T. R., Robinson, M. S., Head, J. W., Strom, R. G., Chapman, C. R., Solomon, S. C., McClintock, W. E., Prockter, L. M., Domingue, D. L., & Blewett, D. T. (2008). Geology of the caloris basin, mercury: A view from MESSENGER. *Science*, *321*(5885), 73–76. https://doi.org/10.1126/science.1159261

Murray, B. C. (1975). The Mariner 10 pictures of Mercury: An overview. *Journal of Geophysical Research*, *80*(17), 2342–2344. https://doi.org/10.1029/JB080i017p02342

Nittler, L. R., Starr, R. D., Weider, S. Z., McCoy, T. J., Boynton, W. V., Ebel, D. S., Ernst, C. M., Evans, L. G., Goldsten, J. O., Hamara, D. K., Lawrence, D. J., McNutt, R. L., Schlemm, C. E., Solomon, S. C., & Sprague, A. L. (2011). The major-element composition of mercury's surface from MESSENGER X-ray spectrometry. *Science*, *333* (6051), 1847–1850. https://doi.org/10.1126/science.1211567

Ostrach, L. R., Robinson, M. S., Whitten, J. L., Fassett, C. I., Strom, R. G., Head, J. W., & Solomon, S. C. (2015). Extent, age, and resurfacing history of the northern smooth plains on Mercury from MESSENGER observations. *Icarus*, *250*, 602–622. https://doi.org/10.1016/j.icarus.2014.11.010

Robinson, M. S., & Lucey, P. G. (1997). Recalibrated Mariner 10 color mosaics: Implications for mercurian volcanism. *Science*, *275*(5297), 197–200. https://doi.org/10.1126/science.275.5297.197

Robinson, M. S., Richard, D. S., Shoshana, Z. W., Timothy, J. M., William, V. B., Denton, S. E., Carolyn, M. E., Larry, G. E., John, O. G., David, K. H., David, J. L., Ralph, L. M., Charles, E. S., Sean, C. S., & Ann, L. S. (2008). Reflectance and color variations on mercury: Regolith processes and compositional heterogeneity. *Science*, *321*(5885), 66–69. https://doi.org/10.1126/science.1160080

Robinson, M. S., & Taylor, G. J. (2001). Ferrous oxide in Mercury's crust and mantle. *Meteoritics & Planetary Science*, *36*(6), 841–847. https://doi.org/10.1111/j.1945-5100.2001.tb01921.x

Solomon, S. C., McNutt, R. L., Watters, T. R., Lawrence, D. J., Feldman, W. C., Head III, J. W., Krimigis Stamatios, M., Murchie Scott, L., Phillips Roger, J., Slavin James, A., & Zuber, M. T. (2008). Return to mercury: A global perspective on MESSENGER's first Mercury flyby. *Science*, *321*(5885), 59–62. https://doi.org/10.1126/science.1159706.

Solomon Sean, C., McNutt Ralph, L., Gold Robert, E., Acuña Mario, H., Baker Daniel, N., Boynton William, V., Chapman Clark, R., Cheng Andrew, F., Gloeckler, G., Head III James, W., Krimigis Stamatios M., Murchie Scott L., Phillips Roger J., Slavin James A., Zuber Maria, T. (2001). The MESSENGER mission to mercury: Scientific objectives and implementation. *Planetary and Space Science*, 49(14–15), 1445–1465. https://doi.org/10.1016/S0032-0633(01)00085-X

Spudis, P. D., & Guest, J. E. (1988). Stratigraphy and geologic history of Mercury. In F. Vilas, C. R. Chapman, & M. S. Matthews (Eds.), *Mercury* (pp. 118–164). University of Arizona Press.

Stepinski, T. F., & Collier, M. L. (2004). Extraction of Martian valley networks from digital topography. *Journal of Geophysical Research*, *109*, 59–62, https://doi.org/10.1029/2004JE002269.

Strom, R. G., Chapman, C. R., Merline, W. J., Solomon, S. C., & Head, J. W. (2008). Mercury cratering record viewed from MESSENGER's first flyby. *Science*, *321*, 79–81. https://doi.org/10.1126/science.1159317.

Strom, R. G., Murray Bruce, C., Belton Michael, J. S., Danielson, G., Edward Davies Merton, E., Gault Donald, E., Hapke, B., O'Leary, B., Trask, N., Guest, J. E., Anderson, J., & Klaasen, K. (1975). Preliminary imaging results from the second mercury encounter. *Journal of Geophysical Research*, *80*(17), 2345–2356. https://doi.org/10.1029/JB080i017p02345

Trask, N. J., & Guest, J. E. (1975). Preliminary geologic terrain map of Mercury. *Journal of Geophysical Research*, *80*(17), 2461–2477. https://doi.org/10.1029/JB080i017p02461

Vander Kaaden, K. E., McCubbin, F. M., Nittler, L. R., Peplowski, P. N., Weider, S. Z., Frank, E. A., & McCoy, T. J. (2017). Geochemistry, mineralogy, and petrology of boninitic and komatiitic rocks on the mercurian surface: Insights into the mercurian mantle. *Icarus*, *285*, 155–168. https://doi.org/10.1016/j.icarus.2016.11.041

Vaz, D. A. (2011). Analysis of a thaumasia planum rift through automatic mapping and strain characterization of normal faults. *Planetary and Space Science*, 1210–1221. https://doi.org/10.1016/j.pss.2010.07.008

Vaz, D. A., Di Achille, G., Barata, M. T., & Alves, E. I. (2012). Tectonic lineament mapping of the thaumasia plateau, Mars: Comparing results from photointerpretation and a semi-automatic approach. *Computers & Geosciences*, *48*, 162–172. https://doi.org/10.1016/j.cageo.2012.05.008

Vaz, D. A., Sarmento, P. T. K., Barata, M. T., Fenton, L. K., & Michaels, T. I. (2015). Object-based dune analysis: Automated dune mapping and pattern characterization for Ganges chasma and Gale crater, Mars. *Geomorphology*, *250*, 128–139. https://doi.org/10.1016/j.geomorph.2015.08.021

Vaz, D. A., & Silvestro, S. (2014). Mapping and characterization of small-scale aeolian structures on Mars: An example from the MSL landing site in Gale Crater. *Icarus*, *230*, 151–161. http://doi.org/10.1016/j.icarus.2013.08.007

Vaz, D. A., Spagnuolo, M. G., & Silvestro, S. (2014). Morphometric and geometric characterization of normal faults on Mars. *Earth and Planetary Science Letters*, *401*, 83–94. https://doi.org/10.1016/j.epsl.2014.05.022

Watters, T. R., & Nimmo, F. (2010). The tectonics of Mercury. In T. R. Watters, & R. A. Schultz (Eds.), *Planetary tectonics* (pp. 15–80). Cambridge University Press.

Watters, T. R., Robinson, M. S., Bina, C. R., & Spudis, P. D. (2004). Thrust faults and the global contraction of mercury. *Geophysical Research Letters*, *31*(4), L04701. https://doi.org/10.1029/2003GL019171

Watters, T. R., Robinson, M. S., & Cook, A. C. (1998). Topography of lobate scarps on Mercury: New constraints on the planet's contraction. *Geology*, *26*(11), 991–994. https://doi.org/10.1130/0091-7613(1998)026<0991:TOLSOM>2.3.CO;2

Watters, T. R., Solomon Sean, C., Robinson Mark, S., Head James, W., André Sarah, L., Hauck Steven, A., & Murchie Scott, L. (2009). The tectonics of Mercury: The view after MESSENGER'S first flyby. *Earth and Planetary Science Letters*, *285*(3-4), 283–296. https://doi.org/10.1016/j.epsl.2009.01.025

Wessel, P., & Smith, W. H. (1998). New, improved version of generic mapping tools released. *Eos, Transactions American Geophysical Union*, *79*(47), 579–579. https://doi.org/10.1029/98EO00426

Wright, J., Rothery, D.A., Balme, M. R., and Conway S. J. (2019), Geology of the hokusai quadrangle (H05), mercury, Journal of Maps, 15(2), 509–520. https://doi.org/10.1080/17445647.2019.1625821